Feasibility study of oxidized naringin as a novel crosslinking agent for crosslinking decellularized porcine Achilles tendon and its potential application for anterior cruciate ligament repair

Can Cheng[1], Xu Peng[2], Linjie Xi[3], Yihao Luo[1], Yuhang Wang[1], Yufan Zhou[1], and Xixun Yu[1]

[1]Sichuan University College of Polymer Science and Engineering
[2]Experimental and Research Animal Institute Sichuan University Chengdu 610065 PR China
[3]Western Theater Command Air Force Hospital Department of Oncology Hematology No 137 Jiuyanqiao shunjiang Road Chengdu Sichuan province 610021 PR China

March 30, 2022

Abstract

Naringin (Nar), a natural flavanone glycoside, has been shown to possess a variety of biological activities, including anti-inflammatory, anti-apoptotic and bone formation, etc. In this study, Nar was oxidized by sodium periodate and the oxidized naringin (ONar) was used as a novel biological crosslinking agent. And ONar-fixed porcine decellularized Achilles tendon (DAT) was developed to substitute anterior cruciate ligament (ACL) for researching a novel ACL replacement materials. The ONar with a 24 h oxidation time had appropriate aldehyde group content, almost no cytotoxicity, and a good crosslinking effect. The critical characteristics and cytocompatibility of ONar-fixed DAT were also investigated. The results demonstrated that 1% ONar-fixed DAT exhibited good resistance to enzymatic degradation and thermal stability as well as suitable mechanical strength. Moreover, 1% ONar-fixed specimens exhibited excellent L929 fibroblasts-cytocompatibility and MC3T3-E1-cytocompatibility. They also promoted the secretion of hepatocyte growth factor (HGF) and basic fibroblast growth factor (bFGF) from fibroblasts and bone morphogenetic protein-2 (BMP-2) from osteoblasts. And they also showed the good anti-inflammatory properties in vivo experiments. Our data provided an experimental basis for ONar as a new cross-linking reagent in chemical modification of DAT and ONar-fixed DAT for ACL repair.

1

Naringin (Nar), a natural flavanone glycoside, has been shown to possess a variety of biological activities, including anti-inflammatory, anti-apoptotic and bone formation, etc. In this study, Nar was oxidized by sodium periodate and the oxidized naringin (ONar) was used as a novel biological crosslinking agent. And ONar-fixed porcine decellularized Achilles tendon (DAT) was developed to substitute anterior cruciate ligament (ACL) for researching a novel ACL replacement materials. The ONar with a 24 h oxidation time had appropriate aldehyde group content, almost no cytotoxicity, and a good crosslinking effect. The critical characteristics and cytocompatibility of ONar-fixed DAT were also investigated. The results demonstrated that 1% ONar-fixed DAT exhibited good resistance to enzymatic degradation and thermal stability as well as suitable mechanical strength. Moreover, 1% ONar-fixed specimens exhibited excellent L929 fibroblasts-cytocompatibility and MC3T3-E1-cytocompatibility. They also promoted the secretion of hepatocyte growth factor (HGF) and basic fibroblast growth factor (bFGF) from fibroblasts and bone morphogenetic protein-2 (BMP-2) from osteoblasts. And they also showed the good anti-inflammatory properties in vivo experiments. Our data provided an experimental basis for ONar as a new cross-linking reagent in chemical modification of DAT and ONar-fixed DAT for ACL repair.

Graphical abstract
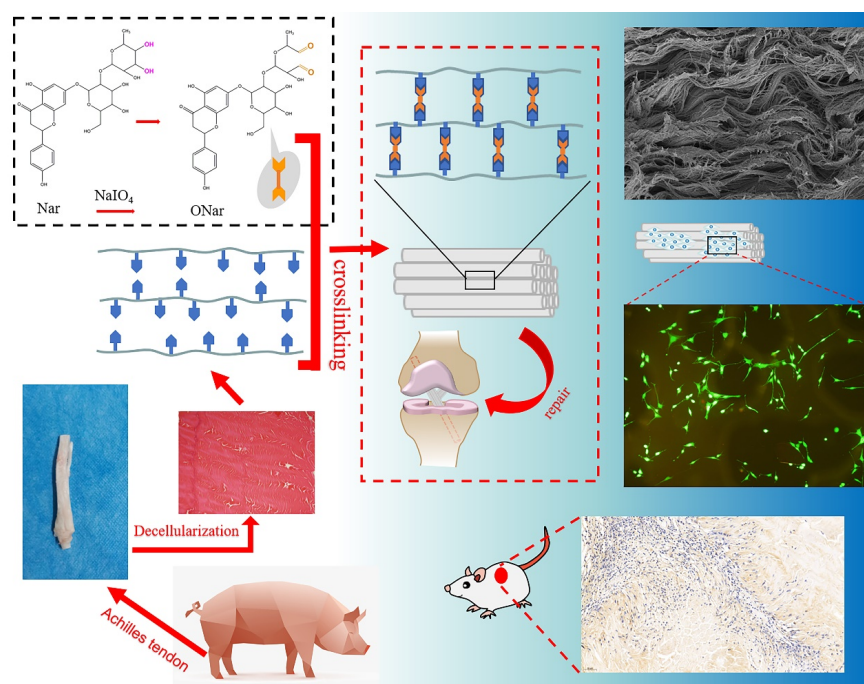
Keywords: oxidized naringin; crosslinking characteristics; decellularized porcine Achilles tendon; anterior cruciate ligament repair.

1. Introduction

The anterior cruciate ligament (ACL) is an important structure of the knee joint, which can provide stability to the knee joint(Zhang, Han, Chen, Wu, & Chen, 2020). For patients with complete ligament rupture and knee joint instability, ACL reconstruction is an indispensable surgical intervention(He et al., 2021). Due to the low degree of vascularization and the limited healing ability of the intra-articular ligaments, simple resuturing is an ineffective repair process. Therefore, grafts are required in ACL reconstruction(Jamil, Ansari, Najabat Ali, & Mir, 2017).

Although the autograft of hamstring and bone patellar tendon bone (BPTB) is currently the gold standard for about 90% ACL reconstruction, it essentially requires additional surgery, which will lead to the morbidity

of the donor site, increased recovery time, and possible pain(Lee et al., 2018). Allogeneic grafts face risks related to limited supply, disease transmission, and host immunogenic response(Y. Li et al., 2020). Synthetic materials are also used for ACL repair, such as poly(L-lactic acid) (PLA)(Silva et al., 2021), polyethylene terephthalate (PET)(Ranger et al., 2011; C.-H. Wang et al., 2015), etc. While, due to the poor biocompatibility, long-term use of synthetic materials can cause knee joint wear, tear and inflammation(J. Chen, Xu, Wang, & Zheng, 2009). An ideal ACL reconstruction material should have the following characteristics: firstly, it has a microstructure similar to ACL extracellular matrix (ECM); secondly, it has bioactivity that could promote the formation of new tissue; thirdly, it has low immunogenicity and similar biomechanical characteristics to ACL(H. Li et al., 2017).

The Achilles tendon (AT) is a dense connective tissue in which a large number of collagen fibers are arranged in parallel in the direction of stress, and it has good mechanical properties(Winnicki, Ochala-Klos, Rutowicz, Pekala, & Tomaszewski, 2020). The internal cellular components of the AT are less, and thus the immunogenicity is low(Ghazanfari, Alberti, Xu, & Khademhosseini, 2019). It is an excellent choice for ACL graft material. After decellularization, the immunogenicity of AT is further reduced, while structural molecules such as collagen and growth factors are retained, providing a microenvironment of the ECM for cell adhesion, growth and differentiation(Ning et al., 2017). However, after decellularization, the resistance to degradation and the mechanical strength of AT are reduced(Cui et al., 2020). In order to overcome these problems, pre-fixation is required to stabilize the tissue structure, reduce biodegradation and maintain its mechanical properties to realize the practical application of biological tissues(X. Wang, Wen, Yang, Li, & Yu, 2017). Fixation is a chemical modification of immobilizing and crosslinking decellularized materials by blocking the binding site of collagenase(X. Wang, Tang, Xu, Yang, & Yu, 2016). At present, a variety of crosslinking reagents have been developed to fix tissues, such as glutaraldehyde (GA)(Yi et al., 2020), genipin(Y. Liu et al., 2019; F. Zhang et al., 2021), etc. Although it can improve the stability of biological tissues, they have many problems in practical applications(Yang, Xie, Ding, Lei, & Wang, 2021). Therefore, we developed a new type of crosslinking agent with lower cytotoxicity which could restore the microstructure of biological tissues and improve their mechanical properties.

Naringin (Nar) is a natural flavanone glycoside which is widely found in citrus plants(R. Chen, Qi, Wang, & Li, 2016; Uchiyama et al., 2008). Studies have shown that Nar has a variety of biological activities, including anti-inflammator(P. Liu, Bian, Fan, Zhong, & Liu, 2020), hepatoprotective(X. Zhang et al., 2021), anti-apoptosis(M. Li et al., 2021), bone formation(Wong & Rabie, 2006), etc. Nar can prevent cyclophosphamide-induced hepatocytes dysfunctions and inflammatory perturbations(Akamo et al., 2021); it can also treat intestinal inflammation caused by nonsteroidal anti-inflammatory drugs (NSAIDs), through accelerate the repair of intestinal mucosa by promoting the secretion of ghrelin and leptin and inhibiting the release of TNF-α(Chao, Dai, & Zhang, 2021); it can also significantly increase the activity of osteoblasts, promote the proliferation of MC3T3-E1 and enhance osteogenic differentiation(L. L. Chen, Lei, Ding, Tang, & Wu, 2011). At the same time, the o-hydroxyl groups in Nar can be oxidized by sodium periodate to dialdehyde groups, which enable oxidized naringin (ONar) to become a new type of biological crosslinking agent(Ding, Zhou, Zeng, Wang, & Shi, 2017). Through Schiff base reaction with amino groups in biological tissues, ONar could improve the stability of biological tissues, and endow the fixed-tissues with anti-inflammatory performance and bone-forming ability.

In this study, to evaluate the feasibility of ONar as a new crosslinking agent, we used ONar to crosslink decellularized porcine Achilles tendon (DAT) and used it as a replacement material for the ACL. We proved the successful oxidation of Nar, and studied the chemical structure, cross-linking characteristics, oxidation degree (the number of aldehyde groups in ONar) and cytotoxicity of ONar. We also investigated the biomechanical properties, ultrastructure, resistance to enzymatic hydrolysis, thermodynamics and cytocompatibility of ONar-fixed DAT. Finally, the histocompatibility of this ONar-fixed DAT in the vivo was evaluated in the research.

2. Materials and methods

2.1 Materials

Nar, GA and Cell Counting Kit-8 (CCK-8) were purchased from Sigma-Aldrich (St. Louis, MO, USA). EDTA and Triton X-100 were obtained from Amresco Co. (USA). DNaseI and RNseA were purchased from Aladdin Co. (Shanghai, China). Fetal bovine serum (FBS) was purchased from Hyclone Laboratories (Logan, UT, USA). Collagenase type I, Roswell Park Memorial Institute-1640 (RPMI-1640), Minimum Essential Medium α (MEM-α), trypsin, penicillin and streptomycin were purchased from Gibcobrl (Grand Island, NY, USA). Analytical grade sodium periodate and all other analytical grade chemicals were purchased from Kelong Co. (Chengdu, China). L929 cells and MC3T3-E1 cells were purchased from West China Hospital, Sichuan University (China).

2.2 Preparation of ONar

ONar was prepared according to our previously reported method(Hu et al., 2021). In short, the Nar () was added in 200 ml distilled water. After heating to dissolve, sodium periodate (equimolar reaction, slight excess of sodium periodate) was added to the solution and then stirred with 600 r/min in dark to predetermined time (6 h, 12 h, 24h, 48h, 72h). The reaction was neutralized by the addition of 10 ml ethylene glycol to reduce the excess periodate. Furthermore, the distilled water was used to dialyze the ONar until there is no periodate in the dialysate (with a molecular weight cutoff of 500). The purified ONar was then lyophilized to obtain the final product.

2.3 Characterization of ONar

The number of aldehyde groups in ONar could be determined by hydroxylamine hydrochloride potentiometric titration(Simon et al., 2022). 0.1 g ONar was dissolved in 25 ml hydroxylamine hydrochloride-methyl orange solution (0.25 mol/L), and the mixed solution was placed in a shaker for 2 h. The hydrochloric acid produced in the mixture was titrated with 0.1 mol/L NaOH standard solution. The titration was discontinued when the color of the solution changed from red to yellow, and the number of aldehyde groups were obtained through the consumed volume of sodium hydroxide. Experiments were made in triplicate.

The chemical structure of Nar and ONar was characterized by Fourier transform infrared (FTIR) and nuclear magnetic resonance (NMR) spectroscopy. For FTIR measurement, 3 mg dried Nar and ONar (72 h) were mixed with 200 mg potassium bromide (KBr) to press into transparent flake under the pressure of 20 MPa. The FTIR spectra were obtained by Nicolet 560, and the data analysis was performed by OMNIC software.

For NMR measurement, Nar and ONar (72 h) were dissolved in NMR tube with a concentration of 10 mg/ml (Nar use DMSO-*d6* and ONar use D_2O). Hydrogen-1 NMR spectrum analysis was performed by a Bruker Avance II-600 MHz NMR instrument.

2.4 Cytotoxicity of ONar

L929 fibroblast cells were used to evaluate the cytotoxicity of ONar in vitro. ONar with different oxidation degree generated by using different reaction time were dissolved in 1640 medium (supplemented with 10% FBS and 1% penicillin-streptomycin). P3 generation L929 fibroblasts were seeded in 96-well culture plates at a cell density of 5×10^4 per ml. After incubated for 24 h, the original medium in every well was discarded and replaced by 100 μl of 400 μg/ml ONar medium, and 100 μl 1640 medium was added to every well in the control group. The cell culture was maintained at 37 with 5% CO_2, with the change of medium every other day. At 1 d, 3 d, 5 d and 7 d, 10 μl (10%) CCK-8 solution was added to each well and incubated in the dark for 60 min at 37 . A microplate reader (model 550, Bio-Rad) was used to record the optical density at 450 nm. The percentage of relative growth rate (RGR) was used to express the cytotoxicity and calculated as follow Eq:

$$\text{RGR } (\%) = \frac{\text{OD}_1}{\text{OD}_0} \times 100\%$$

Where OD_1 is the optical density of cells cultured with ONar with different oxidation degree, and OD_0 is the optical density of cells cultured in the control group. Experiments were made in triplicate.

4

2.5 Decellularization of AT

The fresh porcine AT, which was obtained from the Animal Experiment Center of Sichuan University, was soaked in glycerol and stored at 4 . Phosphate buffered saline (PBS) solution was used to rinse off the blood stains and impurities on the surface of AT before use, and then it was cut into a predetermined size. The prepared AT was immersed in a 4% SDS/PBS solution at 37 for 24 h, and the residual SDS was washed away by PBS solution. Then 1% Triton X-100/PBS solution was used to further decellularize AT for 24 h, after that, PBS solution was used repeatedly to remove the residual decellularization fluid and cell debris.

To analyze the changes of microstructure in AT before and after decellularization, they were embedded in paraffin and sectioned for standard HE staining. A light microscope was employed to observe specimens. Moreover, the DNA, glycosaminoglycan (GAG) in AT and DAT were determined by spectrophotometry with related kits. Finally, the specimens performed by critical point-drying and sputter gold coating were examined by scanning electron microscope (SEM) to observe the fiber structure of AT and DAT.

2.6 Crosslinking of DAT

DAT was soaked in a set of ONar/PBS solution (0.1%; 0.5%; 1%; 2%, m/v), and fixed for 72 h at 37 . 0.625% (v/v) GA was used to crosslink DAT as a control group. Finally, all specimens were washed by PBS solution for 12 h to remove unreacted ONar or GA.

The fixation index (FI) for each crosslinking specimen was determined by ninhydrin color reaction. In short, all crosslinking specimens and DAT (1×1 cm^2) were freeze-dried to constant weight. The lyophilized tissues were immersed in a ninhydrin solution to heat for 20 min. A spectrophotometer was used to measure the absorbance of these solutions at 570 nm. The FI was calculated as follow Eq.:

$$FI\ (\%) = \frac{A_0 - A_1}{A_0} \times 100\%$$

Where A_0 is the absorbance of DAT, and A_1 is the absorbance of the crosslinking specimens. Experiments were made in triplicate.

The residual aldehyde group content for each crosslinking specimen was determined by the glycine-ninhydrin indirect color reaction. Briefly, different concentrations of glycine were added to ninhydrin solution to heat for 20 min, and then the absorbance of these solutions at 570 nm was measured. The glycine standard curve was therefore plotted according to the results above. Secondly, glycine (50μg/ml) was used to react with residual aldehyde groups in fixed specimens, and the residual aldehyde groups were calculated by measuring the consumption of glycine after reaction.

2.7 In vitro enzyme degradation and thermo gravimetric analysis

The enzymatic hydrolytic resistance of the specimens was determined by collagenase hydrolysis. All samples were lyophilized and the initial weights were recorded. Then, they were simultaneously immersed in 1.5 ml of collagenase I/PBS buffer (250U/ml) and were incubated at 37 for a predetermined time (1 h, 3 h, 6 h, 12 h, 24 h). Finally, 10 mM EDTA was added to terminate the enzymatic hydrolysis reaction, and the samples were rinsed with deionized water and lyophilized to weight again. The weight loss percentage ($W\%$) was calculated as follows:

$$W\% = \frac{W_0 - W_t}{W_0} \times 100\%$$

Where W_0 represents the initial weight of the specimen before degradation and W_t represents the weight of the corresponding specimen after degradation.

5

The thermo gravimetric analysis (TGA) was performed on a thermal analyzer (Netzsch TG 209, Germany). 3-8 mg specimens were cut into powder and sealed in aluminum pans and heated. The temperature range was 40 to 600 with a heating rate of 10 /min in N_2 flow. The experiment was performed in triplicate.

2.8 Biomechanical properties

The effect of crosslinking on the biomechanical properties of the specimen was assessed by the Instron material testing machine (Instron Co. USA). Briefly, the specimens with the same fiber arrangement direction were trimmed as a test strap of 4 mm×20 mm in size. The preload of the clamps was 2 MPa, and specimens were extended from 0 g load until the tissue strip ruptured at a constant speed of 5 mm/min. During test, the ultimate load and the ultimate tensile strain were recorded before failure. Experiments were performed in six replicates.

The suture strength was measured with a 2-0 braided polyester suture (Jinhuan Medical Supplies Co. Ltd, Shanghai, China)(Guan et al., 2021). The suture passed through one end of each specimen at 5 mm away from the edge. The suture was then pulled up at a speed of 5 mm/min until it detached from the specimen.

2.9 Cytocompatibility of ONar-fixed specimens

L929 and MC3T3-E1 were employed to evaluate the cytocompatibility of specimens fixed by various concentrations of ONar. L929 cells were cultured in RPMI-1640 medium and MC3T3-E1 cells were cultured in MEM-α medium, which was supplemented with 10% FBS and 1% penicillin-streptomycin. Cells were incubated at 37 with 5% CO_2. The growth medium was replaced every other day and the passages 3 were used for cytocompatibility test. All specimens were sterilized by γ-rays with an irradiation measurement of 25 KGy before test.

2.9.1 Cell proliferation assays

In the cell proliferation experiment, p3 generation of L929 cells (100 µl, 1×10^5 cells/ml) were slowly dropped on the surface of each specimen in the well of 24-well culture plates. After incubation for 3 h, 500 µl serum-containing medium was added to each well. These 24-well plates were incubated at 37 with 5% CO_2, and the medium was changed every other day. After seeding, the cell-specimens were incubated for 1, 3, 5, 7 days. Subsequently, all cell-specimens were transferred to 24-well plates with containing 500 µl of fresh medium and 50 µl of CCK-8 in each well, and incubated for an additional 1 h at 37 . Then, 100 µl of the solution was taken from each well and added to a 96-well plate, and the absorbance was measured at 450 nm using a microplate reader (model 550, Bio-Rad). The RGR of samples was determined according to the method mentioned in chapter 2.4.

A Calcein/PI Live/Dead Viability/Cytotoxicity Assay Kit was used to study the cell viability of L929 and MC3T3-E1 on specimens. Cells were seeded on the surface of the samples with a density of 1×10^5 cells/well. After incubation for 3 days, cells were observed and imaged under fluorescence microscopy (VMF30A).

2.9.2 MC3T3-E1 attachment morphology

In addition, the MC3T3-E1 after incubating for 4 days were selected for observation, specimens were slowly washed with PBS and fixed with 4% paraformaldehyde at 4 for 24 h. Specimens were dehydrated in gradient ethanol (30%, 50%, 70%, 90%, 95%, 98%, and 100%, respectively) at each concentration for 15 min. Finally, cell-loaded samples were critical point-dried and sputter-coated with gold. SEM was employed for the final observation.

2.10 In vitro measurement of protein secretion from cells

The protein secretion of hepatocyte growth factor (HGF) and basic fibroblast growth factor (bFGF) from L929 were quantified using a double ligand enzyme-linked immune sorbent assay (ELISA). Various specimens with attached cells were prepared as detailed above. After the samples were co-cultured with L929 for 4 days, their supernatant liquid was collected and centrifuged at 10000 rpm for 10 min for ELISA assay. A standard curve was plotted according to the measured value of a series concentration of HGF & bFGF

standard solution. Then, the ELISA assay was run according to the manufacturer's instructions (R&D Crop) to determine accurate concentrations of HGF and bFGF.

The bone morphogenetic protein-2 (BMP-2) from MC3T3-E1 was evaluated in the same way as above.

2.11 Immunohistochemical examination

Subcutaneous implantation experiments on rats were carried out to research the anti-inflammation of each specimen. In this study, male rats (200-240 g, n=5) from Chengdu Dashuo Animal Co. Ltd. were used for in vivo assessment, all procedures performed on animals were approved by the Animal Care and Use Committee of Sichuan University. Briefly, the rat was first anesthetized with a respiratory anesthesia machine by isoflurane, all sterilized specimens were implanted on both sides of rat back subcutaneous. The rats were scheduled to be sacrificed by excessive anesthesia at 1 and 3 postoperative months, and the implanted samples were collected and fixed in 4% paraformaldehyde for 24 h. Then fixed specimens were embedded in paraffin and sectioned for immunohistochemical staining (including hematoxylin-eosin (HE) and tumor necrosis factor-α (TNF-α) staining). The data analysis was performed by image-pro plus software 6.0.

2.12 Statistical analysis

Statistical analysis was performed with SPSS (version 20.0). Experimental data was presented as means $\pm$ standard deviation (SD). Results were analyzed by one-way ANOVA with a student's t-test. A p value of $\leq$ 0.05 was considered to be statistically significant.

3. Results and discussion

3.1 Preparation and characterization of ONar

The oxidation of ortho-hydroxyl groups by sodium periodate was determined by the temperature, pH, feed ratio, reaction time, and even light(Coseri et al., 2013). Too high a reaction temperature can lead to the decomposition of sodium periodate, while too low results in a lower reaction rate. pH changes can also seriously affect the oxidation capacity of sodium periodate(Jiang et al., 2016; Ren, Chen, Zhou, & Ji, 2010). Therefore, we control the pH and feeding ratio by equimolar reaction, and the degree of oxidation of ONar was controlled by varying the reaction time. The aldehyde content of ONar can be quickly and accurately determined through hydroxylamine hydrochloride potentiometric titration method. As shown in Figure 1A, with the reaction time increased, the concentration of aldehyde groups in ONar gradually increased. When the reaction time was 6 h, the aldehyde group content was 1.21 mmol/g, however, it reached 2.62 mmol/g when the reaction time was 72 h.

The formation of the dialdehyde groups of ONar was verified by FTIR and NMR spectroscopy(Mozafari, Hojjatoleslamy, & Mohammadizadeh, 2021). As shown in Figure 1B, compared with Nar, the spectrum of ONar (72 h) showed a new characteristic peak at 1750 cm^{-1} that is the most characteristic band of C=O vibrations in aldehyde groups. Besides, a peak at 890 cm^{-1} was present in ONar spectra as well, which could be assigned to the hemiacetal bonds forming between residual aldehyde groups and their neighbor hydroxyl groups(Maroufi, Tabibiazar, Ghorbani, & Jahanban-Esfahlan, 2021). However, due to the existence of the hemiacetal and hydrated aldehydes, the new absorption peak appeared as a weaker shoulder. Nevertheless, the intensity of the peak was still positively correlated with the reaction time. Figure 1C showed the NMR spectra of Nar and ONar. The NMR spectrum of ONar exhibited an aldehyde peak around 9.7 ppm compared with the spectrum of Nar, indicating the successful preparation of ONar(Mozafari et al., 2021).
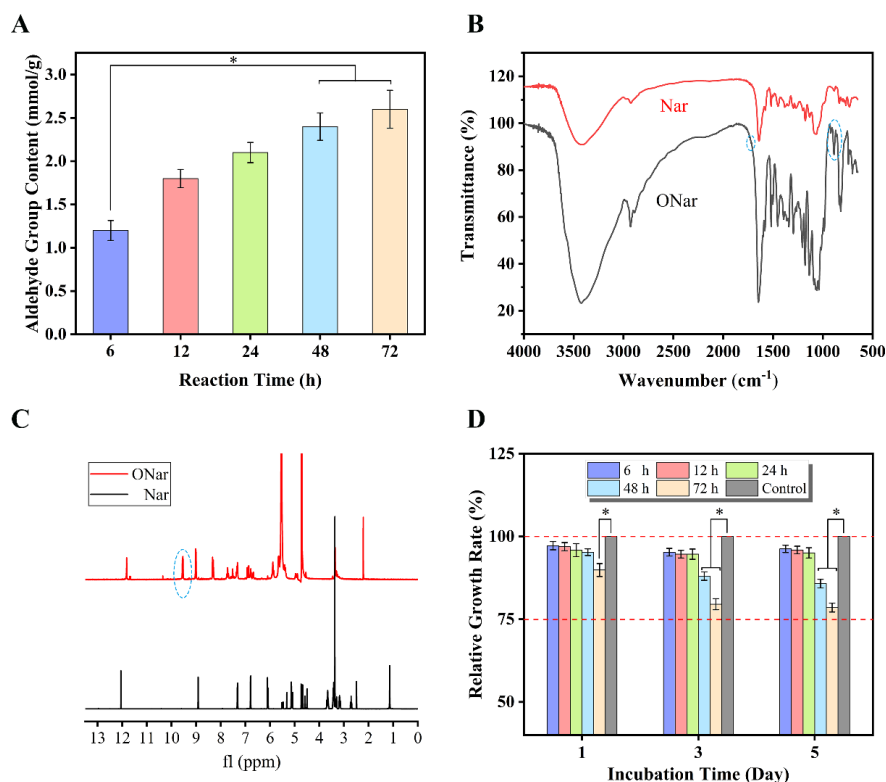
Figure 1. Characterization of ONar (crosslinking agent)

A: aldehyde group content of ONar with different oxidation degree generated by using different reaction time; B: FTIR spectra of Nar and ONar (72 h); C: ^{1}H NMR spectra of Nar and ONar (72 h); D: effect of ONar with different oxidation degree generated by using different reaction time on the relative growth rate of L929 fibroblasts. * represents p < 0.05.

3.2 In vitro cytotoxicity of ONar

The cytotoxicity of ONar was evaluated by the CCK-8 assay. As shown in Figure 1D, the RGR of L929 fibroblasts cultured with ONar suggested that all experimental groups were higher than 75% on the first day. On the 3rd days, 5th days, and 7th days, most of the groups exhibited no cytotoxicity except the ONar-72 and ONar-48 groups. The potent cytotoxicity of the ONar-72 and ONar-48 groups may be correlated with its high aldehyde content. The ONar with a shorter oxidation time showed low cytotoxicity, which might be due to that the smaller number of aldehyde groups in ONar does not affect the good cytocompatibility of this naturally derived glycoside itself. Thus, we chose the ONar with a 24 h oxidation time as a crosslinking reagent for subsequent experiments.

3.3 Decellularization of DAT

In order to systematically evaluate the effect of decellularization, HE staining was performed on DAT and AT, the fiber structures were observed by SEM, and the content of DNA and GAGs were quantitatively determined. As shown in Figure 2A-B, the nuclei were no longer present in DAT samples, but they were present in large quantities in AT specimens. The DNA content in DAT sample (Figure 2E) was significantly reduced to 34±8 ng/mg (459±12 ng/mg for AT sample), meeting the minimum standard for decellularized native tissues (<50 ng/mg)(Z. Liu, Zhu, Zhu, & Tang, 2020). However, we found that the GAG content in DAT (Figure 2F) was only slightly lower than that in AT specimen, indicating that our decellularization protocol only destroyed the cellular structures in the tissue and did not cause damage to the extracellular

8

matrix. It can be seen from the SEM images (Figure 2C-D) that the arrangement direction of fibers remained unchanged, but the space between the fibers increased slightly. This was also confirmed by the HE staining images. Thus, the decellularization method we used can effectively remove cellular components, reduce immune antigenicity, and maintain an integral structure of ECM.
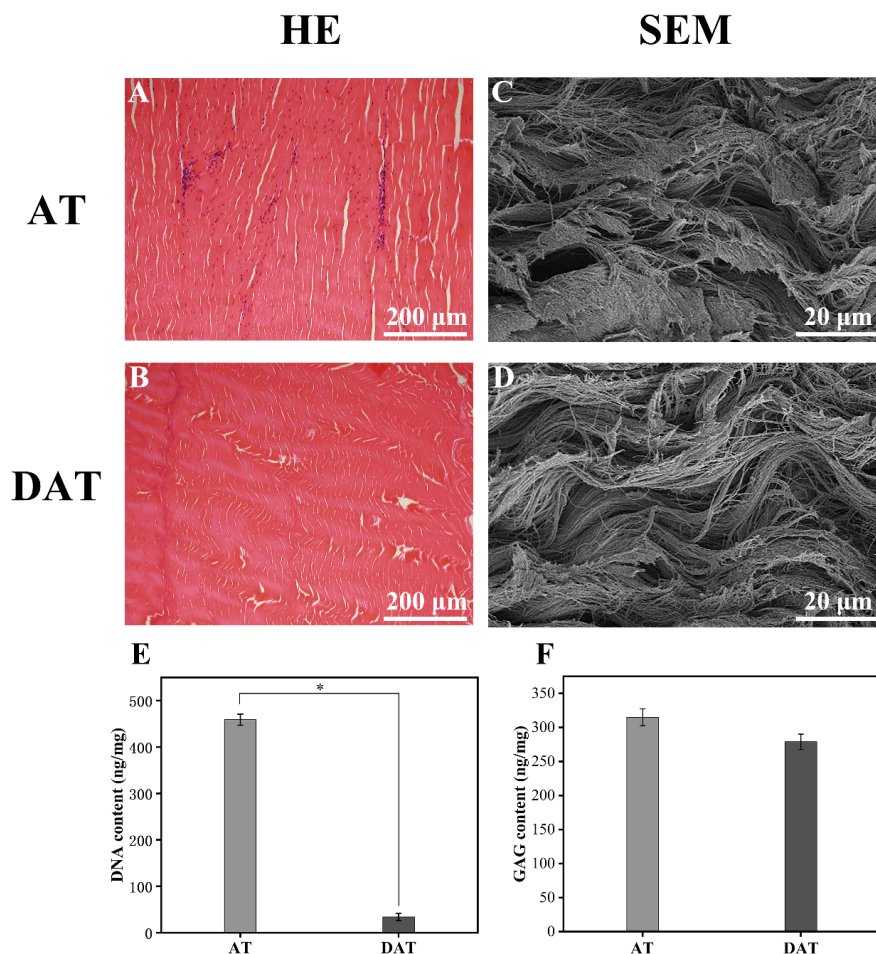

Figure 2. Characterization of decellularization of AT and DAT.

A-B: standard H&E stain for AT and DAT; C-D: SEM images for AT and DAT; E: DNA content; F: GAG content. * represents p < 0.05.

3.4 The fixation of DAT

The fixation index (FI) was used to estimate the amount of free amino groups left in tissues, to further quantitatively evaluate the degree of the crosslinking reaction. Generally, a higher FI indicates fewer free amino groups residual in fixed tissues and reveals a higher degree of crosslinking. As shown in Figure 3A, the FI of 0.1% ONar fixed DAT was only 38.38, which might be due to that the lower concentration of aldehyde in 0.1% ONar only reacted with a small fraction of amino group within the tissues and left a number of free amino groups in tissues. However, with the increase of ONar's concentration, the corresponding FI gradually increased, and the crosslinking reaction gradually reached peak. The maximum FI (84.74) of fixed sample could be achieved when the concentration of ONar was 2%, which was already close to that of glutaraldehyde fixed samples (88.27). This indicated that ONar could be used as a new crosslinking agent and achieve a good effect of crosslinking.

9

There were some residual aldehyde groups on the surface of specimens after crosslinking, which could reduce the cytocompatibility of samples. These residual aldehyde groups mainly came from two sources: the aldehyde groups in the crosslinking agent that had not reacted with amino groups within tissues; and the aldehyde groups released from reversible Schiff reaction between the aldehyde groups and the amino group. However, the aldehyde groups produced by the reverse reaction were negligible due to the forward reaction of Schiff reaction equilibrium. It can be seen from Figure 3B that the residual aldehyde group content in DAT specimens fixed by lower concentration of ONar was less. While the residual aldehyde group content in 2% ONar-fixed DAT samples was significantly higher. The reason for this is that there were no more sites in the superficial tissues of DAT to react with the aldehyde group due to the high concentration of ONar, resulting in the remaining of some crosslinkers on the surface of DAT through physical adsorption. Similarly, glutaraldehyde was easily physically absorbed on the surface of DAT due to its low molecular weight, which eventually also led to a high content of residual aldehyde groups in GA-fixed specimens.

3.5 In vitro enzymatic hydrolysis

One of the main purposes of biological tissue fixation is to avoid too rapid degradation and extend storage time(He et al., 2021; Z. Li et al., 2015). Therefore, it is necessary to assess the resistance of fixed tissues to enzymatic degradation.

As illustrated in Figure 3C, the relative weight loss of tested specimens all increased significantly with the hydrolysis time. Alternatively, compared to crosslinked tissues, the DAT degraded more rapidly and extensively during the whole hydrolysis process. It was obvious that the DAT was hydrolyzed by 10.60% after the initial degradation period (3 h) and were hydrolyzed by 80.62% after 24 h of enzymatic digestion, while 1% and 2% ONar-fixed specimens were hydrolyzed only 32.44% and 25.26% respectively even after 24 h of enzymatic degradation. This indicated that a certain concentration of ONar crosslinked DAT had ideal resistance against enzymatic degradation. In the early stage, a large number of stable covalent bonds were formed through crosslinking reaction between the aldehyde group in the ONar and the free amino group within tissue, leading to the hiding or obstructing of most of the enzyme-attacked sites on collagen, which could effectively prevent rapid degradation to provide sufficient mechanical support and substitute partial functions of original host anterior cruciate ligament after graft-implantation in the early stage. The enzymatic degradation rate of ONar-fixed DAT was also found to be concentration-dependent and increased with the decrease in ONar concentration, which also validated the conclusion discussed above that the higher crosslinking degree, the better stability of the tissue. To sum up, ONar could be a promising crosslinking agent to construct the graft for anterior cruciate ligament.

3.6 Thermal stability

TGA was an effective method used to characterize the thermal stability of specimens(Magli et al., 2021). The temperature at the maximum mass loss rate ($T_{\max}$) calculated from DTG curves was corresponded to the decomposition temperature of the specimen(Hivechi, Hajir Bahrami, & Siegel, 2019). From Figure 3D, it could be seen that the weight loss of the specimens gradually decreased and the $T_{\max}$ increased with the increase of ONar concentration, indicating that the thermal stability of the samples was improved after crosslinking. The $T_{\max}$ of 2% ONar-fixed DAT reached at 319 , which was 8 higher than that of the DAT (311). This is due to that the stable covalent bond structure formed by ONar fixation in DAT could improve the stability of the specimen, making it require more energy to break the bonds and decompose during thermal decomposition. This was consistent with the results of in vitro enzymatic hydrolysis, which further indicated the success of the crosslinking.
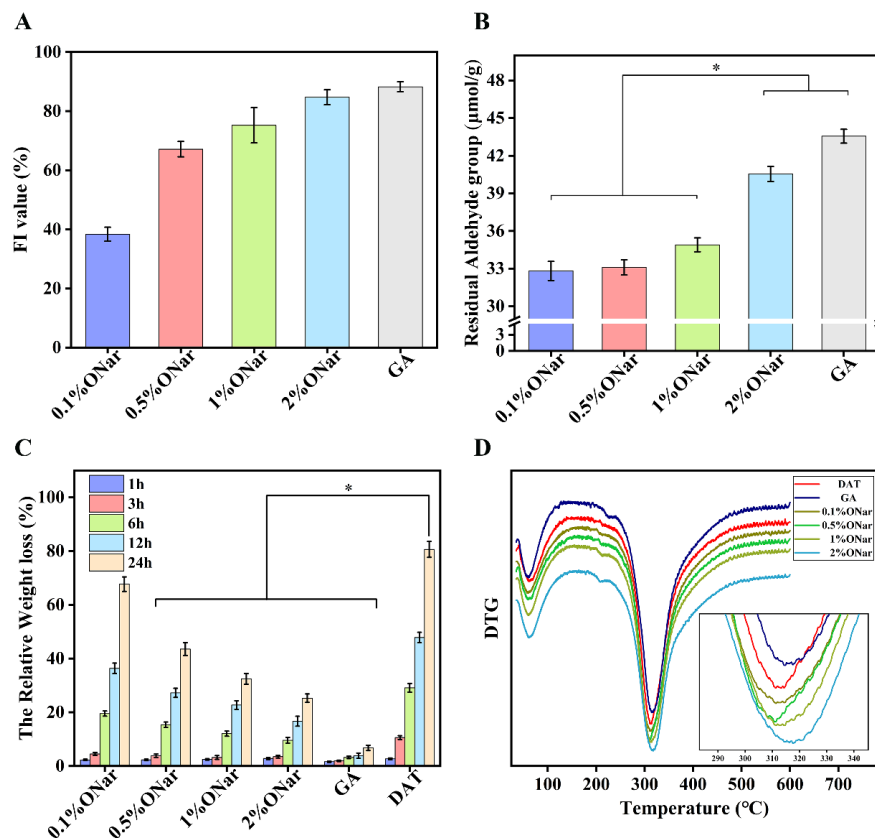
10

Figure 3. Characterization of physical and chemical properties for DAT and difference crosslinked specimens.

A: FI of DAT fixed with GA and various concentrations of ONar; B: residual aldehyde content for various specimens; C: in vitro enzymatic hydrolysis in collagenase for each sample; D: DTG curve for various specimens. * represents p < 0.05.

3.7 Biomechanical properties

Maintaining knee stability and supporting lower extremity motion are inextricably linked to the mechanical properties of the ACL(de la Garza-Castro et al., 2017). Therefore, as a replacement material for ACL, ONar-fixed DAT also needs to have sufficient biomechanical strength. Figure 4 showed the biomechanical properties of DAT, 0.1%-2% ONar-fixed DAT, and GA-fixed DAT. Compared with the DAT, the biomechanical strength of ONar-fixed specimens was significantly improved. 2% ONar-fixed DAT achieved a failure load of 703 N, which was much higher than the 173 N of DAT (Figure 4A). However, the failure load of GA-fixed DAT reached to 975N due to the brittleness and hardness of fixed samples resulting from fiber denaturation caused by GA fixation. The data on modulus (Figure 4B) also showed that the modulus of specimens was significantly improved after crosslinking, which was because the crosslinking agent could promote the formation of a complex interwoven network between the collagen fibers by forming stable covalent bonds within tissue, which could improve the modulus of the fixed specimens.

The suture strength of specimens was measured considering the practical clinical application as the ACL replacement materials(Shi et al., 2019). As shown in Figure 4C-D, the tear strength of all fixed samples was significantly higher than that of DAT (30N). With the increase of ONar concentration, the tear strength of fixed samples gradually increased from about 40 N of 0.1% ONar-fixed DAT to about 60 N of 2% ONar-fixed DAT. This indicated that the ONar fixation could improve the tear strength of specimens, which was

11

beneficial for the application of ONar-fixed DAT in the replacement of ACL.
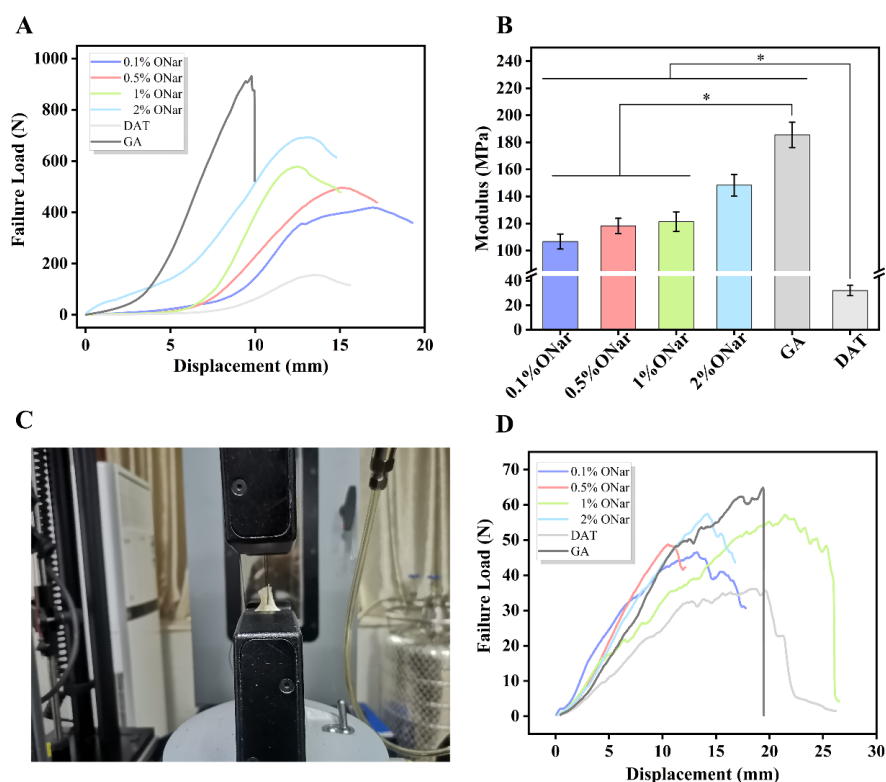

Figure 4 . Biomechanical performance of DAT, 0.1%-2% ONar- and GA-fixed DAT.

A: load-displacement curve of samples; B: modulus of various specimens; C-D: schematic diagram of suture strength test and its load-displacement curve. * represents p < 0.05.

3.8 In vitro cytocompatibility

3.8.1 Cell proliferation assays

In order to assess the cytocompatibility of fixed DAT, the fibroblasts were cultured on samples and the viability of these cells was measured using CCK-8 assay(Kuang et al., 2019). The results are shown in Figure 5A, both DAT and GA-fixed DAT inhibited the proliferation of L929 fibroblasts, while ONar-fixed DAT exhibited better cell proliferation. On the 3rd day, 5th day and 7th day, the RGR of L929 cultured on ONar-fixed groups were all higher than 80%, and L929 grown on 1% ONar group showed the highest RGR, indicating its excellent cytocompatibility. As mentioned above, DAT specimens degraded rapidly, and the substances from degradation exhibited cytotoxicity and inhibited cell growth, while, the GA-fixed samples presented severe cytotoxicity due to its low molecular weight with high content of residual aldehyde groups and the continuous leaching-out of the unreacted GA. For ONar-fixed samples, ONar fixation could improve the resistance of the specimen to enzymatic degradation, leading to few degradation products with cytotoxicity released from fixed samples; moreover, ONar derived from natural glycosides exhibited high cytocompatibility in itself(Cao, Feng, & Kan, 2021).

The morphology of L929 fibroblasts cultured with specimens for 3 days by Calcein AM/PI fluorescent staining was shown in Figure 5B. The cells on ONar-fixed specimens showed better cell viability, which was consistent with the results of CCK-8 assay.
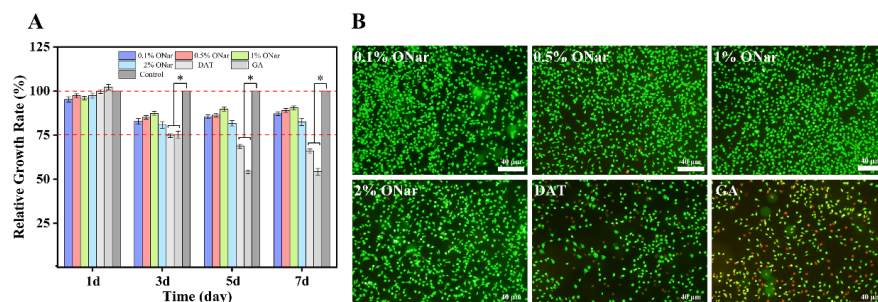
12

Figure 5. In vitro cytocompatibility of DAT, 0.1%-2% ONar- and GA-fixed DAT.

A: effects of DAT, 0.1%-2% ONar- and GA-fixed DAT on relative growth rate of L929 fibroblasts on 1 d, 3 d, 5 d and 7 d; B: cell viability of L929 fibroblasts was determined by Calcein/PI Live/Dead Viability/Cytotoxicity Assay Kit. * represents p < 0.05.

3.8.2 MC3T3-E1 morphology observation

During the reconstruction of the ACL, peri-tunnel bone formation was close to fracture healing process, we investigated the effect of the specimens on osteoblasts by co-culturing the samples with MC3T3-E1.

We evaluated the viability of MC3T3-E1 grown on samples using the same method as above, and as seen in Figure 6, the cells on the surface of ONar-fixed specimens exhibited better cell viability, which was similar to the case of L929 fibroblasts.
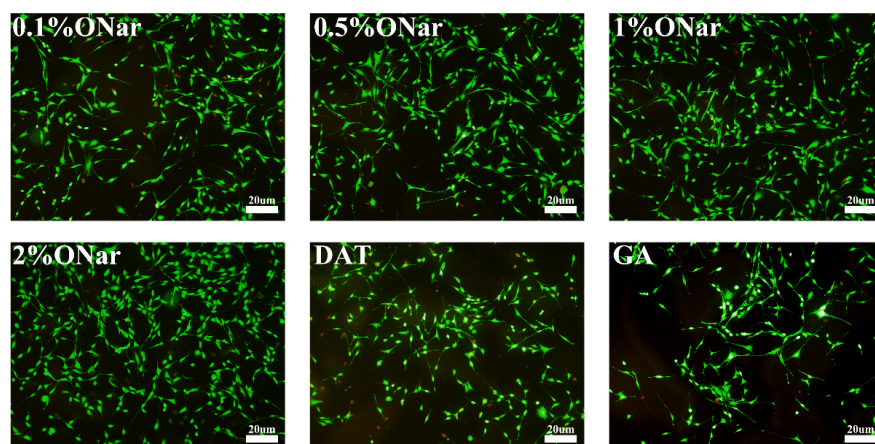

Figure 6 . Cell viability of MC3T3-E1 cells on various specimens.

The proliferation and spread of MC3T3-E1 on the surface of each specimen was observed under SEM to further evaluate their cytocompatibilities. As shown in Figure 7, on the surface of GA-fixed DAT, fewer scattered cells with rounded shape were observed, which is characteristic of poor cytocompatibility of samples. In contrast, the cells on DAT fixed with different concentrations of ONar grew better, all of which were their characteristic polygonal squamous and fully spread. The MC3T3-E1 on the surface of DAT fixed by 0.5% and 1% ONar appeared to grow much better and nearly reached the continuous cell layer with osteoblasts growing in the direction of the fiber of the specimens. The result was consistent with the live-dead staining assay.
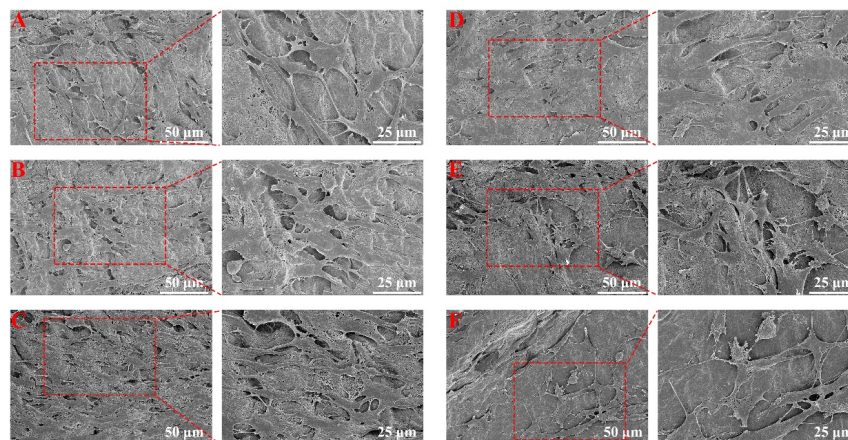
13

Figure 7. SEM for MC3T3-E1 cultured on samples.

(A) 0.1% ONar; (B) 0.5% ONar; (C) 1% ONar; (D) 2% ONar; (E) DAT; (F) GA

3.9 Secretion of growth factors from cells on fixed specimens

The process of reconstructing ACL using biodegradable materials is complex, which involves a variety of cells and growth factors that contribute to improving cell function(R. Wang et al., 2021). HGF and bFGF are two cell growth factors that play an important role in the healing process of ACL. HGF can promote the adhesive healing process at the tendon-bone junction, both histologically and mechanically in ligament reconstruction model(Nakase, Kitaoka, Matsumoto, & Tomita, 2010). The ability of bFGF to improve cellular architecture, promote new bone formation and enhance the mechanical properties of ligaments contributes to the healing process after ACL reconstruction(B. Chen et al., 2016). The test results of HGF and bFGF are shown in Figure 8A-B. The amount of HGF and bFGF secreted from L929 fibroblasts on ONar-fixed specimens were significantly higher than those from cells on DAT and GA-fixed groups. This is because the secretion of HGF and bFGF was positively correlated with the number and viability of L929 fibroblasts on various samples, among which ONar-fixed specimens showed better cytocompatibility (resulting in high number and viability of L929 fibroblasts on samples). In short, the secretion of HGF and bFGF from cells grown on ONar-fixed samples could be promoted, which facilitated the reconstruction of ACL.

BMP-2 is an osteoinductive factor that promotes bone regeneration and osseointegration(Hettiaratchi et al., 2017). It can be found from Figure 8D that the amount of BMP-2 secreted from MC3T3-E1 grown on ONar-fixed samples were significantly higher than that on DAT and GA-fixed DAT, and the highest BMP-2 expression was found in 1% ONar-fixed group. The results might be due to: ONar-fixed samples were less cytotoxic and able to promote osteoblasts proliferation versus DAT and GA-fixed samples, then there were more cells to secrete BMP-2 on ONar-fixed samples than that on DAT and GA-fixed samples; therefore, the amounts of BMP- culture medium could be enhanced in ONar-fixed groups. In addition, in previous studies, naringin has been found to promote osteoblast proliferation. We speculated that oxidized naringin still had the ability to promote osteoblast proliferation, which also led to the high expression of BMP- ONar-fixed groups. Based on this, we concluded that ONar-fixed DAT could better promote the proliferation and activation of osteoblasts, which is beneficial for ACL reconstruction.

Based on above cytocompatibility results, 1% ONar-fixed DAT was chosen for subsequent animal experiments in this study.
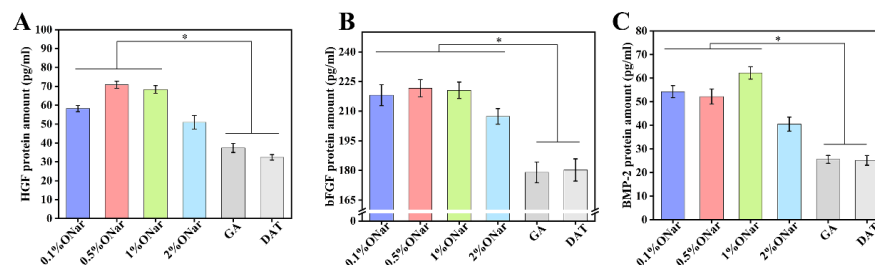
14

Figure 8. The secretion of cytokine from L929 fibroblasts and MC3T3-E1 on various samples.

A: HGF for L929 fibroblasts; B: bFGF for L929 fibroblasts; C: BMP-2 for MC3T3-E1 cells. * represents p < 0.05.

3.10 Animal study

The excellent histocompatibility of implant materials could ensure their clinical safety when they are used as ACL replacement materials(He et al., 2021). In order to evaluate the histocompatibility and inflammatory response of specimens, we performed immunohistochemical staining (H&E and TNF-α) on all harvested samples. After specimens are implanted subcutaneously in rats, a certain degree of inflammatory response will occur around implants, and these appropriate inflammatory reactions could promote wound healing(Crawford, Wyatt, Bryers, & Ratner, 2021). The results of H&E staining were shown in Figure 9, at 4 postoperative weeks, a small amount of neovascularization could be seen around samples in DAT group, but samples showed more degradation, which was not conducive to the reconstruction of ACL. In GA-fixed group, a large number of inflammatory cells were observed surrounding test samples, which was not conducive to tissue repair. For ONar-fixed group, no significant degradation of the specimens was found, while the migration of surrounding tissue cells to the interior of the ONar-fixed DAT and the formation of neovascularization could be observed, and the number of inflammatory cells around samples was fewer. At 12 postoperative weeks, the infiltration of inflammatory cells in all specimens was reduced, while DAT was degraded severely, the inflammation of GA-fixed specimen was still more serious than ONar-fixed samples. In conclusion, ONar-fixed specimens showed excellent biocompatibility.
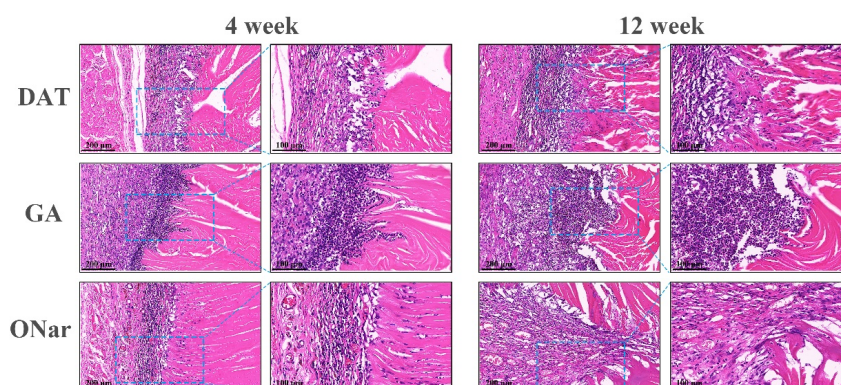

Figure 9. H&E immunohistochemical analysis for various implanted specimens in vivo.

The ACL replacement materials need to ensure a lower inflammatory response after implantation(Szychlinska et al., 2020). TNF-α is a cytokine released by immune cells that can reflect the degree of inflammation and further attract and activate inflammatory cells(Zysk et al., 2004). The results of immunohistochemical staining of TNF-α for each specimen were shown in Figure 10. At the early stage of sample implantation

(4 W), all groups showed a more pronounced inflammatory response, which was due to the large amount of TNF-α released from macrophages activated classically by samples during early implantation. While, after 12 weeks of implantation, TNF-α could be found to be still highly expressed both in DAT group and GA-fixed group, indicating that there was still a severe inflammatory response at implantation site. And the excessive concentration of TNF-α could have a counter-regulatory effect on the wound healing. However, the TNF-α expression around ONar-fixed specimens significantly decreased after 12 weeks of implantation. This indicated the good anti-inflammatory properties of ONar-fixed specimens due to the anti-inflammatory of Naringin, leading to better tissue repairs at the implantation site of ONar-fixed specimens.
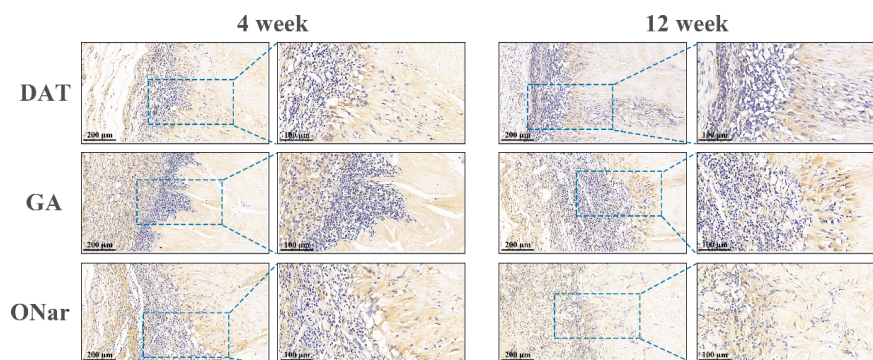

Figure 10. TNF-α immunohistochemical analysis for various implanted specimens in vivo.

4. Conclusion

In summary, we successfully designed a new type of crosslinking agent: oxidized naringin (ONar), and used it for crosslinking porcine decellularized Achilles tendon (DAT) to prepare a potential replacement material for ACL. ONar with a 24 h oxidation time which had appropriate aldehyde group content and low cytotoxicity was used as a crosslinking agent to modify DAT. The ONar-fixed DAT exhibited good resistance to enzymatic degradation and thermal stability as well as suitable mechanical strength. Moreover, these specimens exhibited excellent cytocompatibility in vitro and were able to stimulate the secretion of HGF and bFGF from L929 fibroblasts inoculated on the surface of ONar-fixed DAT, as well as the secretion of BMP-2 from MC3T3-E1 on ONar-fixed samples, which facilitated the reconstruction of ACL. The ONar-fixed samples also exhibited slight inflammatory reactions and excellent histocompatibility in vivo. This study provides the experimental basis for ONar as a new cross-linking reagent in chemical modification of DAT for ACL replacement materials.

Author contributions

Can Cheng: Conceptualization, Methodology, Data curation, Writing-original draft. **Xu Peng:** Investigation, Visualization.**Linjie Xi:** Investigation, Data curation. **Yihao Luo:**Methodology, Software. **Yuhang Wang:** Investigation, Formal analysis. **Yufan Zhou:** Investigation, Formal analysis.**Xixun Yu:** Funding acquisition, Writing-review & editing, Supervision.

Acknowledgements

Data availability statement: The data that support the findings of this study are available from the corresponding author upon reasonable request.

Compliance with ethical standards

Conflict of interest: The authors declares that they have no conflict of interest.

Ethical approval: All institutional and national guidelines for the care and use of laboratory animals were followed.

References

Akamo, A. J., Rotimi, S. O., Akinloye, D. I., Ugbaja, R. N., Adeleye, O. O., Dosumu, O. A., . . . Cole, O. E. (2021). Naringin prevents cyclophosphamide-induced hepatotoxicity in rats by attenuating oxidative stress, fibrosis, and inflammation. *Food Chem Toxicol, 153*, 112266. doi:10.1016/j.fct.2021.112266 Cao, W., Feng, S. J., & Kan, M. C. (2021). Naringin Targets NFKB1 to Alleviate Oxygen-Glucose Deprivation/Reoxygenation-Induced Injury in PC12 Cells Via Modulating HIF-1alpha/AKT/mTOR-Signaling Pathway. *J Mol Neurosci, 71*(1), 101-111. doi:10.1007/s12031-020-01630-8 Chao, G., Dai, J., & Zhang, S. (2021). Protective effect of naringin on small intestine injury in NSAIDs related enteropathy by regulating ghrelin/GHS-R signaling pathway. *Life Sci, 266*, 118909. doi:10.1016/j.lfs.2020.118909 Chen, B., Li, B., Qi, Y. J., Ni, Q. B., Pan, Z. Q., Wang, H., & Chen, L. B. (2016). Enhancement of tendon-to-bone healing after anterior cruciate ligament reconstruction using bone marrow-derived mesenchymal stem cells genetically modified with bFGF/BMP2. *Sci Rep, 6*, 25940. doi:10.1038/srep25940 Chen, J., Xu, J., Wang, A., & Zheng, M. (2009). Scaffolds for tendon and ligament repair: review of the efficacy of commercial products. *Expert Rev Med Devices, 6*(1), 61-73. doi:10.1586/17434440.6.1.61 Chen, L. L., Lei, L. H., Ding, P. H., Tang, Q., & Wu, Y. M. (2011). Osteogenic effect of Drynariae rhizoma extracts and Naringin on MC3T3-E1 cells and an induced rat alveolar bone resorption model. *Arch Oral Biol, 56*(12), 1655-1662. doi:10.1016/j.archoralbio.2011.06.008 Chen, R., Qi, Q. L., Wang, M. T., & Li, Q. Y. (2016). Therapeutic potential of naringin: an overview. *Pharm Biol, 54*(12), 3203-3210. doi:10.1080/13880209.2016.1216131 Coseri, S., Biliuta, G., Simionescu, B. C., Stana-Kleinschek, K., Ribitsch, V., & Harabagiu, V. (2013). Oxidized cellulose–survey of the most recent achievements. *Carbohydr Polym, 93*(1), 207-215. doi:10.1016/j.carbpol.2012.03.086 Crawford, L., Wyatt, M., Bryers, J., & Ratner, B. (2021). Biocompatibility Evolves: Phenomenology to Toxicology to Regeneration. *Adv Healthc Mater, 10*(11), e2002153. doi:10.1002/adhm.202002153 Cui, J., Ning, L. J., Yao, X., Zhang, Y., Zhang, Y. J., He, S. K., . . . Qin, T. W. (2020). Influence of the integrity of tendinous membrane and fascicle on biomechanical characteristics of tendon-derived scaffolds. *Biomed Mater, 16*(1), 015029. doi:10.1088/1748-605X/abc203 de la Garza-Castro, S., Gonzalez-Rivera, C. E., Vilchez-Cavazos, F., Morales-Avalos, R., Barrera-Flores, F. J., Elizondo-Omana, R. E., . . . Mendoza-Lemus, O. F. (2017). Clinical, biomechanical and morphological assessment of anterior cruciate ligament Kevlar(R)-based artificial prosthesis in rabbit model. *J Appl Biomater Funct Mater, 15*(3), e251-e261. doi:10.5301/jabfm.5000353 Ding, W., Zhou, J., Zeng, Y., Wang, Y. N., & Shi, B. (2017). Preparation of oxidized sodium alginate with different molecular weights and its application for crosslinking collagen fiber. *Carbohydr Polym, 157*, 1650-1656. doi:10.1016/j.carbpol.2016.11.045 Ghazanfari, S., Alberti, K. A., Xu, Q., & Khademhosseini, A. (2019). Evaluation of an elastic decellularized tendon-derived scaffold for the vascular tissue engineering application. *J Biomed Mater Res A, 107*(6), 1225-1234. doi:10.1002/jbm.a.36622 Guan, G., Yu, C., Fang, X., Guidoin, R., King, M. W., Wang, H., & Wang, L. (2021). Exploration into practical significance of integral water permeability of textile vascular grafts. *J Appl Biomater Funct Mater, 19*, 22808000211014007. doi:10.1177/22808000211014007 He, X., Li, Y., Guo, J., Xu, J., Zu, H., Huang, L., . . . Qin, L. (2021). Biomaterials developed for facilitating healing outcome after anterior cruciate ligament reconstruction: Efficacy, surgical protocols, and assessments using preclinical animal models. *Biomaterials, 269*, 120625. doi:10.1016/j.biomaterials.2020.120625 Hettiaratchi, M. H., Rouse, T., Chou, C., Krishnan, L., Stevens, H. Y., Li, M. A., . . . Guldberg, R. E. (2017). Enhanced in vivo retention of low dose BMP-2 via heparin microparticle delivery does not accelerate bone healing in a critically sized femoral defect. *Acta Biomater, 59*, 21-32. doi:10.1016/j.actbio.2017.06.028 Hivechi, A., Hajir Bahrami, S., & Siegel, R. A. (2019). Investigation of morphological, mechanical and biological properties of cellulose nanocrystal reinforced electrospun gelatin nanofibers. *Int J Biol Macromol, 124*, 411-417. doi:10.1016/j.ijbiomac.2018.11.214 Hu, M., Peng, X., Zhao, Y., Yu, X., Cheng, C., & Yu, X. (2021). Dialdehyde pectin-crosslinked and hirudin-loaded decellularized porcine pericardium with improved matrix stability, enhanced anti-calcification and anticoagulant for bioprosthetic heart valves. *Biomater Sci, 9*(22), 7617-7635. doi:10.1039/d1bm01297e Jamil,

T., Ansari, U., Najabat Ali, M., & Mir, M. (2017). A Review on Biomechanical and Treatment Aspects Associated with Anterior Cruciate Ligament. *Irbm, 38*(1), 13-25. doi:10.1016/j.irbm.2016.10.002 Jiang, X., Yang, Z., Peng, Y., Han, B., Li, Z., Li, X., & Liu, W. (2016). Preparation, characterization and feasibility study of dialdehyde carboxymethyl cellulose as a novel crosslinking reagent.*Carbohydr Polym, 137*, 632-641. doi:10.1016/j.carbpol.2015.10.078 Kuang, M. J., Zhang, W. H., He, W. W., Sun, L., Ma, J. X., Wang, D., & Ma, X. L. (2019). Naringin regulates bone metabolism in glucocorticoid-induced osteonecrosis of the femoral head via the Akt/Bad signal cascades. *Chem Biol Interact, 304*, 97-105. doi:10.1016/j.cbi.2019.03.008 Lee, K. I., Lee, J. S., Kang, K. T., Shim, Y. B., Kim, Y. S., Jang, J. W., . . . D'Lima, D. D. (2018). In Vitro and In Vivo Performance of Tissue-Engineered Tendons for Anterior Cruciate Ligament Reconstruction.*Am J Sports Med, 46*(7), 1641-1649. doi:10.1177/0363546518759729 Li, H., Li, J., Jiang, J., Lv, F., Chang, J., Chen, S., & Wu, C. (2017). An osteogenesis/angiogenesis-stimulation artificial ligament for anterior cruciate ligament reconstruction. *Acta Biomater, 54*, 399-410. doi:10.1016/j.actbio.2017.03.014 Li, M., Liu, J., Liu, D., Duan, X., Zhang, Q., Wang, D., . . . Lu, Z. (2021). Naringin attenuates cisplatin- and aminoglycoside-induced hair cell injury in the zebrafish lateral line via multiple pathways. *J Cell Mol Med, 25*(2), 975-989. doi:10.1111/jcmm.16158 Li, Y., Zhu, T., Wang, L., Jiang, J., Xie, G., Huangfu, X., . . . Zhao, J. (2020). Tissue-Engineered Decellularized Allografts for Anterior Cruciate Ligament Reconstruction. *ACS Biomater Sci Eng, 6*(10), 5700-5710. doi:10.1021/acsbiomaterials.0c00269 Li, Z., He, J., Li, X., Bian, W., Zhang, W., Li, D., . . . Snedeker, J. G. (2015). Regeneration Of Anterior Cruciate Ligament with Silk-Based Scaffold In Porcine Model. *Journal of Mechanics in Medicine and Biology, 15*(01). doi:10.1142/s0219519415500062 Liu, P., Bian, Y., Fan, Y., Zhong, J., & Liu, Z. (2020). Protective Effect of Naringin on In Vitro Gut-Vascular Barrier Disruption of Intestinal Microvascular Endothelial Cells Induced by TNF-alpha. *J Agric Food Chem, 68*(1), 168-175. doi:10.1021/acs.jafc.9b06347 Liu, Y., Cai, Z., Sheng, L., Ma, M., Xu, Q., & Jin, Y. (2019). Structure-property of crosslinked chitosan/silica composite films modified by genipin and glutaraldehyde under alkaline conditions.*Carbohydr Polym, 215*, 348-357. doi:10.1016/j.carbpol.2019.04.001 Liu, Z., Zhu, X., Zhu, T., & Tang, R. (2020). Evaluation of a Biocomposite Mesh Modified with Decellularized Human Amniotic Membrane for Intraperitoneal Onlay Mesh Repair. *Acs Omega, 5*(7), 3550-3562. doi:10.1021/acsomega.9b03866 Magli, S., Rossi, L., Consentino, C., Bertini, S., Nicotra, F., & Russo, L. (2021). Combined Analytical Approaches to Standardize and Characterize Biomaterials Formulations: Application to Chitosan-Gelatin Cross-Linked Hydrogels. *Biomolecules, 11*(5). doi:10.3390/biom11050683 Maroufi, L. Y., Tabibiazar, M., Ghorbani, M., & Jahanban-Esfahlan, A. (2021). Fabrication and characterization of novel antibacterial chitosan/dialdehyde guar gum hydrogels containing pomegranate peel extract for active food packaging application. *Int J Biol Macromol, 187*, 179-188. doi:10.1016/j.ijbiomac.2021.07.126 Mozafari, H., Hojjatoleslamy, M., & Mohammadizadeh, M. (2021). Optimizing the properties of Zodo gum and examining its potential for amino acid binding by periodate oxidation. *Int J Biol Macromol, 167*, 1517-1526. doi:10.1016/j.ijbiomac.2020.11.106 Nakase, J., Kitaoka, K., Matsumoto, K., & Tomita, K. (2010). Facilitated tendon-bone healing by local delivery of recombinant hepatocyte growth factor in rabbits. *Arthroscopy, 26*(1), 84-90. doi:10.1016/j.arthro.2009.06.029 Ning, L. J., Jiang, Y. L., Zhang, C. H., Zhang, Y., Yang, J. L., Cui, J., . . . Qin, T. W. (2017). Fabrication and characterization of a decellularized bovine tendon sheet for tendon reconstruction. *J Biomed Mater Res A, 105*(8), 2299-2311. doi:10.1002/jbm.a.36083 Ranger, P., Renaud, A., Phan, P., Dahan, P., De Oliveira, E., Jr., & Delisle, J. (2011). Evaluation of reconstructive surgery using artificial ligaments in 71 acute knee dislocations. *Int Orthop, 35*(10), 1477-1482. doi:10.1007/s00264-010-1154-x Ren, Q. G., Chen, S. Y., Zhou, X. T., & Ji, H. B. (2010). Highly efficient controllable oxidation of alcohols to aldehydes and acids with sodium periodate catalyzed by water-soluble metalloporphyrins as biomimetic catalyst. *Bioorg Med Chem, 18*(23), 8144-8149. doi:10.1016/j.bmc.2010.10.026 Shi, F. D., Hess, D. E., Zuo, J. Z., Liu, S. J., Wang, X. C., Zhang, Y., . . . Hu, W. N. (2019). Peroneus Longus Tendon Autograft is a Safe and Effective Alternative for Anterior Cruciate Ligament Reconstruction.*J Knee Surg, 32*(8), 804-811. doi:10.1055/s-0038-1669951 Silva, M., Gomes, C., Pinho, I., Goncalves, H., Vale, A. C., Covas, J. A., . . . Paiva, M. C. (2021). Poly(Lactic Acid)/Graphite Nanoplatelet Nanocomposite Filaments for Ligament Scaffolds. *Nanomaterials (Basel), 11*(11). doi:10.3390/nano11112796 Simon, J., Tsetsgee, O., Iqbal, N. A., Sapkota, J., Ristolainen, M., Rosenau, T., & Potthast, A. (2022). Fourier transform and near infrared dataset of

18

dialdehyde celluloses used to determine the degree of oxidation with chemometric analysis. *Data Brief, 40*, 107757. doi:10.1016/j.dib.2021.107757 Szychlinska, M. A., Calabrese, G., Ravalli, S., Dolcimascolo, A., Castrogiovanni, P., Fabbi, C., . . . Musumeci, G. (2020). Evaluation of a Cell-Free Collagen Type I-Based Scaffold for Articular Cartilage Regeneration in an Orthotopic Rat Model. *Materials (Basel), 13*(10). doi:10.3390/ma13102369 Uchiyama, N., Kim, I. H., Kikura-Hanajiri, R., Kawahara, N., Konishi, T., & Goda, Y. (2008). HPLC separation of naringin, neohesperidin and their C-2 epimers in commercial samples and herbal medicines. *J Pharm Biomed Anal, 46*(5), 864-869. doi:10.1016/j.jpba.2007.04.004 Wang, C.-H., Guo, Z.-S., Pang, F., Zhang, L.-Y., Yan, M., Yan, J.-H., . . . Han, Y.-S. (2015). Effects of Graphene Modification on the Bioactivation of Polyethylene-Terephthalate-Based Artificial Ligaments. *ACS Applied Materials & Interfaces, 7*(28), 15263-15276. doi:10.1021/acsami.5b02893 Wang, R., Wu, G., Dai, T., Lang, Y., Chi, Z., Yang, S., & Dong, D. (2021). Naringin attenuates renal interstitial fibrosis by regulating the TGF-beta/Smad signaling pathway and inflammation. *Exp Ther Med, 21*(1), 66. doi:10.3892/etm.2020.9498 Wang, X., Tang, P., Xu, Y., Yang, X., & Yu, X. (2016). In vitro study of strontium doped calcium polyphosphate-modified arteries fixed by dialdehyde carboxymethyl cellulose for vascular scaffolds. *Int J Biol Macromol, 93*(Pt B), 1583-1590. doi:10.1016/j.ijbiomac.2016.04.047 Wang, X., Wen, K. L., Yang, X., Li, L., & Yu, X. X. (2017). Biocompatibility and anti-calcification of a biological artery immobilized with naturally-occurring phytic acid as the crosslinking agent. *Journal Of Materials Chemistry B, 5*(40), 8115-8124. doi:10.1039/c7tb02090b Winnicki, K., Ochala-Klos, A., Rutowicz, B., Pekala, P. A., & Tomaszewski, K. A. (2020). Functional anatomy, histology and biomechanics of the human Achilles tendon - A comprehensive review. *Ann Anat, 229*, 151461. doi:10.1016/j.aanat.2020.151461 Wong, R. W., & Rabie, A. B. (2006). Effect of naringin collagen graft on bone formation. *Biomaterials, 27*(9), 1824-1831. doi:10.1016/j.biomaterials.2005.11.009 Yang, L., Xie, S., Ding, K., Lei, Y., & Wang, Y. (2021). The study of dry biological valve crosslinked with a combination of carbodiimide and polyphenol. *Regen Biomater, 8*(1), rbaa049. doi:10.1093/rb/rbaa049 Yi, S., Huh, M. I., Hong, H., Yoon, D., Park, H. S., Kim, D. S., & Kim, H. K. (2020). Development of Contact Lens-Shaped Crosslinked Amniotic Membranes for Sutureless Fixation in the Treatment of Ocular Surface Diseases. *Transl Vis Sci Technol, 9*(6), 12. doi:10.1167/tvst.9.6.12 Zhang, F., Zhang, N., Xu, Q., Zhang, L., Zhang, C., Liu, H., . . . Huang, F. (2021). Decellularized nerve extracellular matrix/chitosan crosslinked by genipin to prepare a moldable nerve repair material. *Cell Tissue Bank, 22*(3), 419-430. doi:10.1007/s10561-020-09889-2 Zhang, P., Han, F., Chen, T., Wu, Z., & Chen, S. (2020). "Swiss roll"-like bioactive hybrid scaffolds for promoting bone tissue ingrowth and tendon-bone healing after anterior cruciate ligament reconstruction. *Biomater Sci, 8*(3), 871-883. doi:10.1039/c9bm01703h Zhang, X., Zhang, Y., Gao, W., Guo, Z., Wang, K., Liu, S., . . . Chen, Y. (2021). Naringin improves lipid metabolism in a tissue-engineered liver model of NAFLD and the underlying mechanisms. *Life Sci, 277*, 119487. doi:10.1016/j.lfs.2021.119487 Zysk, S. P., Fraunberger, P., Veihelmann, A., Dorger, M., Kalteis, T., Maier, M., . . . Refior, H. J. (2004). Tunnel enlargement and changes in synovial fluid cytokine profile following anterior cruciate ligament reconstruction with patellar tendon and hamstring tendon autografts. *Knee Surg Sports Traumatol Arthrosc, 12*(2), 98-103. doi:10.1007/s00167-003-0426-z

HE   **SEM**

AT

DAT

A

B

C

D

A

B

C

D